BCSJ

Document type: Article

Copper(II) Complexes of 10,20-Diaryl-5,15-diazaporphyrin: Alternative Synthesis, Excited State Dynamics, and Substituent Effect on the $^1O_2$-Generation Efficiency

Hikari Ochiai,[1] Tomoaki Miura,[2] Tadaaki Ikoma,[2] Mao Minoura,[3] Haruyuki Nakano,[4] and Yoshihiro Matano*[2]

[1]Department of Fundamental Sciences, Graduate School of Science and Technology, Niigata University, Nishi-ku, Niigata 950-2181, Japan

[2]Department of Chemistry, Faculty of Science, Niigata University, Nishi-ku, Niigata 950-2181, Japan

[3]Department of Chemistry, College of Science, Rikkyo University, Toshima-ku, Tokyo 171-8501, Japan

[4]Department of Chemistry, Graduate School of Science, Kyushu University, Nishi-ku, Fukuoka 819-0395, Japan

E-mail: matano@chem.sc.niigata-u.ac.jp

Received: January 5, 2022; Accepted: January 25, 2022; Web Released: February 1, 2022

Yoshihiro Matano

Yoshihiro Matano was appointed Assistant Professor at the Faculty of Science, Kyoto University in 1990 and received his Ph.D. degree from Kyoto University in 1994 under the supervision of Professor Hitomi Suzuki. He moved to the Graduate School of Engineering, Kyoto University in 2002 as an Associate Professor, and to the Faculty of Science, Niigata University in 2013 as a Full Professor. His research interests include main group element chemistry and porphyrin chemistry.

Abstract

The synthesis, excited state dynamics, and substituent effect on the $^1O_2$-generation efficiency of several copper(II) complexes of 5,15-diazaporphyrin (CuDAPs) bearing peripheral substituents are reported. 10,20-Diaryl-CuDAPs were prepared via a new method consisting of metal-templated cyclization and *N*-dealkylation as key steps. The effect of the β-substituents on the optical and redox properties of CuDAP was stronger than that of the *meso*-aryl groups, which can be explained by considering the characteristics of the HOMO and LUMO of the DAP ring. The excited state dynamics and $^1O_2$-generation efficiency of CuDAPs were studied using time-resolved spectroscopic techniques; the electronic effect of the *meso*-aryl groups on the triplet lifetime and $^1O_2$-generation quantum yield was relatively weak, whereas that of the β-(1-pyrazolyl) groups was appreciable. The analysis of the temperature dependence of phosphorescence spectra of 10,20-bis(2,4,6-trimethylphenyl)-CuDAP allowed the energy gap between the excited trip-quartet and trip-doublet states to be determined. The relatively long triplet lifetimes of CuDAPs show their potential for future application as photosensitizers.

Keywords: Diazaporphyrin | Copper | Singlet oxygen

1. Introduction

The photosensitized production of singlet oxygen ($^1O_2$) is known as a Type-II reaction in photodynamic therapy (PDT), and its efficiency depends on the excited state dynamics of sensitizers. Metalloporphyrins with sufficiently long triplet lifetimes (τ_T) and high $^1O_2$-generation quantum yields (Φ_Δ) have been typically used as sensitizers in PDT.[1] However, precious heavy metals such as palladium and platinum are often necessary to facilitate the singlet–triplet intersystem-crossing process. Therefore, it is of practical importance to explore porphyrin complexes that use abundant and low-cost metals for use as sensitizers for application in PDT. 5,15-Diazaporphyrins (DAPs), including **P1**–**P3** (Chart 1), are potential PDT sensitizers[2–5] because they exhibit high performance in the Type-II reaction under irradiation of visible light of long wavelength and, in some instances, near infrared (NIR) light. In our recent

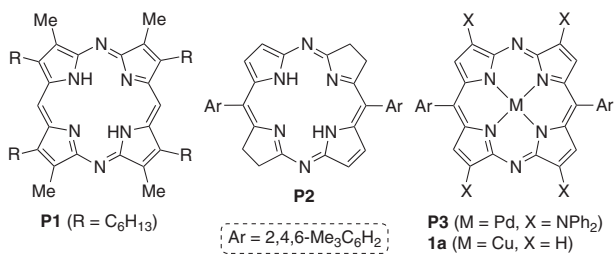

Chart 1. DAP derivatives **P1**–**P3** and CuDAP **1a**.

study, we observed that the copper(II) complex of 10,20-dimesityl-DAP **1a** (mesityl = 2,4,6-trimethylphenyl) emitted phosphorescence and produced $^1O_2$ with high Φ_Δ in toluene at room temperature.[5b] These results verified the applicability of CuDAPs as a PDT sensitizer and prompted us to investigate the effects of the peripheral substituents on the triplet lifetime and $^1O_2$-generation efficiency of CuDAPs.

Most of the known CuDAPs have been prepared by metal-templated cyclization reactions of copper(II)–bis(1,9-dibromodipyrrin) complexes with sodium or copper(I) azide under diluted conditions.[6,7] However, this method requires inherently explosive metal azides, and its experimental protocol is typically laborious owing to the use of a large amount of solvents, such as *N*,*N*-dimethylformamide (DMF). Herein, we report a new method for the synthesis of 10,20-diaryl-CuDAPs, with metal-templated cyclization and *N*-dealkylation as key steps. The effects of the peripheral substituents of CuDAPs on their optical and redox properties, triplet lifetime, and $^1O_2$-generation efficiency are also reported.

2. Results and Discussion

The synthesis of 10,20-diaryl-CuDAPs **1** is shown in Scheme 1. The reaction of 1,9-dichloro-5-mesityldipyrrin **2a** with β-alanine methyl ester, generated from **3A**, yielded 1-chloro-5-mesityl-9-(2-methoxycarbonylethyl)aminodipyrrin **4aA**, which then underwent metal-templated cyclization by treatment with copper(II) acetate in CH_2Cl_2–MeOH to give 19π 5,15-bis(2-methoxycarbonylethyl)-10,20-dimesityl-CuDAP **5aA**. From the results of a separate study on water-soluble CuDAPs,[8] we predicted that alkali hydrolysis of two ester groups in **5aA** would produce a CuDAP derivative bearing 2-carboxyethyl groups at the 5,15-positions. However, the treatment of **5aA** with NaOH in EtOH–H_2O at 60 °C resulted in *N*-dealkylation, yielding **1a** as the major product. This unexpected finding suggested that a similar protocol would be practical for the synthesis of **1b**, **c**. The treatment of **4bA** and **4cA**, available from **2b**, **c** and **3A**, with $Cu(OAc)_2$ afforded the corresponding 19π radical cations **5bA** and **5cA**, respectively, as air-stable solids. The base-promoted *N*-dealkylation of **5bA** gave **1b**, whereas that of **5cA** produced **1d**, not **1c**, via alkali hydrolysis of the *para*-ester moieties of the 10,20-diaryl groups.

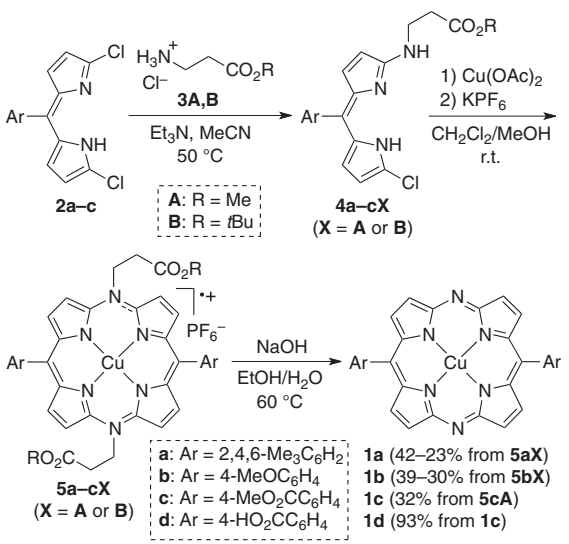

Scheme 1. Synthesis of 10,20-diaryl-CuDAPs **1a–d**.

Plausible reaction mechanisms for the *N*-dealkylation of **5**, a Hofmann-type elimination and a stepwise hydrolysis–decarboxylative fragmentation, are shown in Scheme S1 in the Supporting Information.[9] Compounds **5aB**, **5bB**, and **5cB** were obtained via the corresponding precursors **4aB**, **4bB**, and **4cB**, respectively, when **3B** was used instead of **3A**. The *N*-dealkylation of **5aB**, **5bB**, and **5cB** with NaOH in EtOH–H_2O produced **1a**, **1b**, and **1d**, respectively. Compound **1c** was independently prepared from **4cA** via the esterification of **1d**. (for details, see the Supporting Information). The synthetic protocol shown in Scheme 1 has practical advantages over the known methods, in that it precludes the use of intrinsically explosive metal azides and a large amount of DMF. To reveal the electronic effect of the β-substituents, **1a** was converted to 3,7,13,17-tetrasubstituted derivatives **6** and **7** by regioselective bromination with *N*-bromosuccinimide (NBS)[7c] and direct amination with pyrazole/NaOH,[5a] respectively (Scheme 2).

The newly prepared CuDAP derivatives were characterized by high-resolution electrospray ionization (ESI) mass spectrometry, infrared spectroscopy, and ultraviolet–visible–NIR (UV–vis–NIR) absorption spectroscopy. The crystal structure of **5cA** was unambiguously elucidated using X-ray crystallography. As shown in Figure 1, **5cA** possesses a slightly ruffled DAP π-plane, wherein the copper center adopts a square planar geometry with the average $Cu–N_{core}$ bond length of 1.98 Å. The two *meso*-aryl groups are considerably twisted against the DAP ring with dihedral angles of 51.6° and 83.3°.

The UV–vis–NIR absorption spectra of the CuDAP derivatives are shown in Figures 2 and S1, and the optical data for **1a–d**, **6**, and **7** are summarized in Table 1. Compounds **1a–d** exhibited intense Q bands at absorption maxima (λ_{max}) of 578–580 nm, where the marginal electronic effect of the *meso*-aryl groups was detected. The peripheral β-substitution with bromine atoms or 1-pyrazolyl groups shifted the Q band of **1a** (λ_{max} = 578 nm) to longer wavelengths by 16 and 48 nm, respectively. In the UV–vis–NIR absorption spectra of the 19π radical cations **5** in CH_2Cl_2, the lowest-energy π–π* transitions appeared in the NIR region with λ_{max} of 875–882 nm.

The redox potentials of the CuDAP derivatives in CH_2Cl_2 were measured through cyclic voltammetry with Bu_4NPF_6 as a supporting electrolyte, and the results are summarized in Figure S2 and Table S2. The electronic effect of the *meso*-substituents on the redox potentials of the DAP ring was weak, whereas that of the β-substituents was strong. The positive shifts in the 18π/19π redox processes of **6** and **7** vs. **1a**

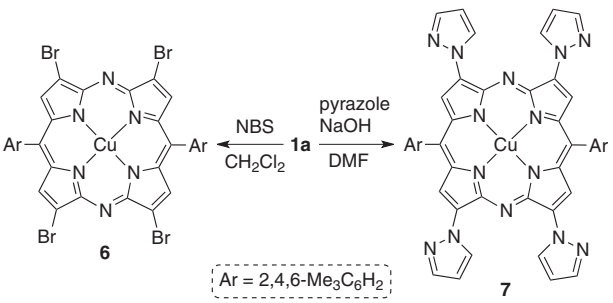

Scheme 2. Synthesis of CuDAPs **6** and **7** from **1a**.

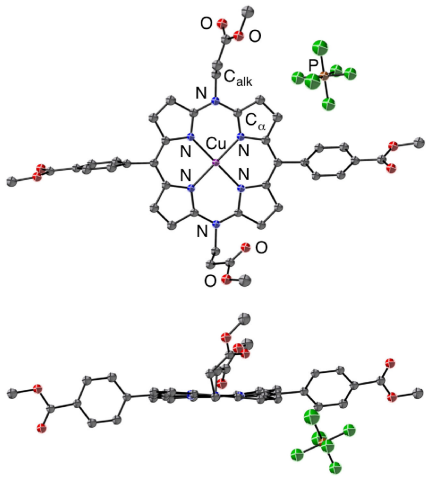

Figure 1. Top and side views (50% probability ellipsoids) of **5cA**. Hydrogen atoms are omitted for clarity. Selected bond lengths (Å): Cu–N_{core} 1.972(1)–1.986(1); N_{meso}–C_α 1.367(2)–1.373(2); N_{meso}–C_{alk} 1.487(2)–1.488(2).

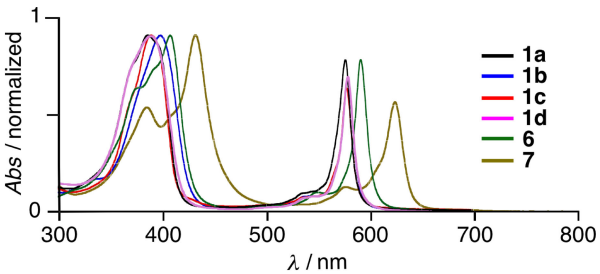

Figure 2. UV–vis absorption spectra of **1a**–**c**, **6**, and **7** in toluene and **1d** in MeOH.

Table 1. Optical and photophysical properties[a)]

DAP	λ_a[b)]	τ_{T0} (τ_T)/μs[c)]	Φ_Δ[d)]	λ_P[e)]	τ_{P0} (τ_P)/μs[f)]
1a[g)]	578	1.30 (0.40)	0.69	849	1.47 (0.43)
1b	580	1.21 (0.31)	0.74	847	1.45 (0.33)
1c	580	1.70 (0.34)	0.80	847	1.97 (0.39)
1d	579	0.17 (0.11)	0.35	n.d.	n.d.
6	594	1.34 (0.38)	0.72	n.d.	n.d.
7	626	0.31 (0.21)	0.32	n.d.	n.d.

a) Measured in toluene (**1a**–**c**, **6**, **7**) or MeOH (**1d**) at 298 K. n.d. = not determined. b) Absorption maxima in nm. c) Triplet lifetimes under Ar-saturated condition. Data in parentheses are those under air-saturated condition. d) O_2-quenching quantum yield under air-saturated condition. $\Phi_\Delta = k_q[O_2]/(1/\tau_T)$. $k_q[O_2] = (1/\tau_T) - (1/\tau_{T0})$. e) Emission maxima in nm. f) Phosphorescence lifetimes under Ar-saturated condition. Data in parentheses are those under air-saturated condition. g) Data from ref. 5b.

($\Delta E_{1/2} = +0.27$ and $+0.24$ V, respectively) were larger than those in the 18π/17π redox processes of **6** and **7** vs. **1a** ($\Delta E_{1/2} = +0.21$ and $+0.02$ V, respectively), implying that these β-substituents exert a stronger influence on the LUMO energy than that on the HOMO energy of the DAP ring. The electrochemical HOMO–LUMO gaps of **1a** (2.14 eV), **6** (2.08 eV), and **7** (1.92 eV) were very close to the optical HOMO–LUMO gaps estimated from their absorption spectra.

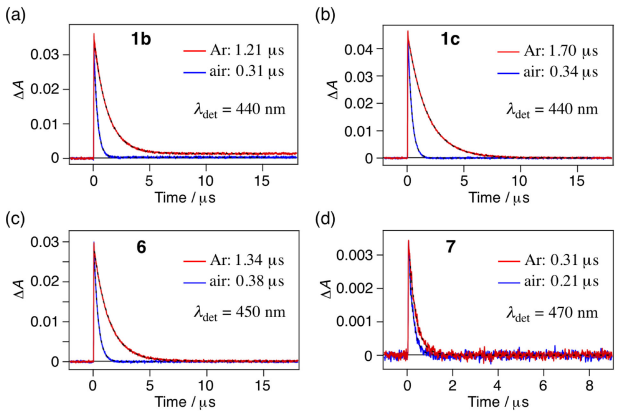

Figure 3. Kinetic traces and their fittings for the T_1 state of (a) **1b**, (b) **1c**, (c) **6**, and (d) **7** in Ar- or air-saturated condition at indicated times. Measured in toluene at room temperature. $\lambda_{ex} = 532$ nm. Triplet lifetimes and detection wavelengths (λ_{det}) are indicated. The transient absorption spectra and kinetic traces for **1a** are reported in ref. 5b.

To clarify the substituent effects of CuDAPs on their excited state dynamics, we first measured the transient absorption of **1b**–**d**, **6**, and **7** in toluene at 298 K. The results are summarized in Figure 3 and Table 1. Upon the irradiation of a sample solution with a Nd:YAG laser ($\lambda_{ex} = 532$ nm), transient absorption bands promptly appeared in the wavelength range where there was no absorption of the ground state for CuDAPs, all of which exhibited single-exponential decay profiles. The lifetimes of the transient species under air-saturated conditions (τ_T) were significantly shorter than those under Ar-saturated conditions (τ_{T0}). Based on these results, the transient species were assigned to the excited triplet (T_1) state of the DAPs as observed for **1a**. This finding was also supported by the fact that **1a**–**c** emitted phosphorescence (Figure S3) with very similar lifetimes. Among the β-unsubstituted CuDAPs, **1c** exhibited the longest triplet lifetime ($\tau_{T0} = 1.7$ μs) and the highest $^1O_2$-generation efficiency ($\Phi_\Delta = 0.80$). In contrast, both τ_T and Φ_Δ values of the *para*-carboxy derivative **1d** were considerably lower than those of **1c** although their HOMO–LUMO gaps were almost identical. When dimethyl sulfoxide was used instead of MeOH, the lifetime of the transient species generated from **1d** was too short for reliable analysis. Therefore, it is likely that the solvated structure of **1d** differs from that of **1c**; **1d** might aggregate in solution owing to its ambipolar character. Assuming that the O_2 concentration is the same for all samples except for **1d**, which was measured in the different solvents, the O_2-quenching rate constant (k_q) of **1a** ($k_q[O_2] = 1.7 \times 10^6\ s^{-1}$) is rather smaller than that of **1b** and **1c** (each, $k_q[O_2] = 2.4 \times 10^6\ s^{-1}$). This may come from steric congestion around the metal center in the mesityl derivative **1a**. The τ_{T0} and ϕ_Δ values of **6** were close to those of **1a**, indicating the marginal heavy-atom effect of the four bromine atoms bound to the pyrrolic-β positions on the excited state dynamics of CuDAP. In contrast, the appreciably low τ_{T0} and Φ_Δ values of **7** may stem from the diminished HOMO–LUMO gap owing to effective π-conjugation between the pyrazole and DAP rings.

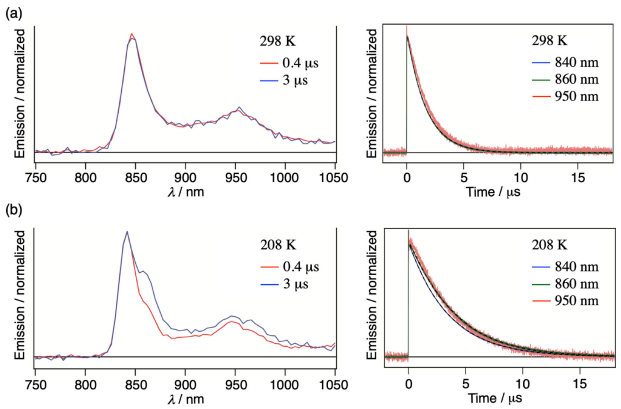

Figure 4. Emission spectra of **1a** in toluene and kinetic traces at (a) 298 K and (b) 208 K. $\lambda_{ex} = 532$ nm.

The different effects of the β substituents on the energy transfer process are evident from k_q of **6** ($k_q[O_2] = 1.9 \times 10^6\ s^{-1}$) and **7** ($k_q[O_2] = 1.5 \times 10^6\ s^{-1}$).

We also examined the chemical detection of $^1O_2$ (Figure S4) by irradiating a toluene solution containing CuDAP and 1,3-diphenylisobenzofuran (a $^1O_2$ quencher) with visible light ($\lambda_{ex} = 540$ nm). The $^1O_2$-generation quantum yields obtained for **1c** ($\Phi_\Delta = 0.86$) and **7** ($\Phi_\Delta = 0.45$) were comparable to those determined by transient absorption spectroscopy (Table 1). It is worth noting that the prolongation of τ_{T0} of **1c** and **7** enabled them to excite $^3O_2$ much more efficiently than CuTPP ($\Phi_\Delta <$ 0.1; CuTPP = 5,10,15,20-tetraphenylporphyrinatocopper(II)).[10]

The relaxation processes of excited copper(II) porphyrins (CuPs) have been studied in relation to substituent effects.[10,11] For example, Asano et al. point out the important role of the orbitals of CuPs for the dynamics of the T_1 state; the peripheral substituents exert a significant impact on the energy gap (ΔE_T) between the lowest trip-quartet ($^4T_1$) and trip-doublet ($^2T_1$) states, which is related to the thermal activation from the ^4T to the ^2T state.[10] Notably, the τ_{T0} values of **1a–c** are significantly longer than those of the CuPs.[12] This is in contrast to the results found on zinc(II) complexes of the fully β-substituted DAP and porphyrin,[13] implying key roles of the copper(II) center and *meso*-substituents in the excited state dynamics of **1a–c**. To gain a deeper insight into the excited state dynamics of CuDAPs, we measured temperature dependence of the phosphorescence of **1a** in toluene. The phosphorescence spectrum at 298 K had the intense 0-0 band at 849 nm and decayed exponentially with a rate constant (k_{decay}) of $5.9 \times 10^5\ s^{-1}$ as shown in Figure 4a. At 208 K, the 0-0 band split into two peaks with an energy gap (ΔE_T) of ca. 280 cm^{-1}, which was probably caused by spectral narrowing and suppression of the non-radiative transition at the low temperature (Figure 4b). The strong 0-0 band at 840 nm and the weak 0-0 band at 860 nm can be assigned to emissions from the $^2T_1$ and $^4T_1$ states, respectively, based on the spin selection rule in the radiative transition to the ground doublet ($^2S_0$) state. Both the strong and weak 0-0 bands decayed exponentially with the same k_{decay} of $2.9 \times 10^5\ s^{-1}$. In addition, the kinetics of the weak 0-0 band included a small component rising with a rate constant of $4 \times 10^5\ s^{-1}$. The same decay rate for the two bands of spin allowed and forbidden transitions suggests interconversion between the $^2T_1$ and the $^4T_1$ states. The observed rise of the weak band might reflect a process approaching a steady state of the interconversion. The Arrhenius analysis of k_{decay} over the temperature range 298–188 K (Figure S5) clarified an activation energy (E_a) of 310 cm^{-1} for the decay of the $^2T_1$ state. The good agreement between E_a and ΔE_T values supports the efficient reverse intersystem crossing from the $^4T_1$ to the $^2T_1$ state, as illustrated in Figure 5.

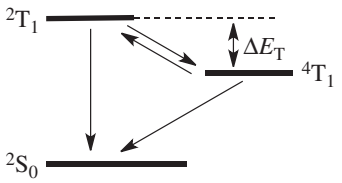

Figure 5. A schematic diagram of the excited triplet states of **1a**.

High $^1O_2$-generation efficiency obtained by the photosensitization of CuDAPs originates from the long lifetimes of their T_1 states at room temperature, which are considerably longer than those of CuPs such as CuTPP ($\tau_{T0} = 29$ ns) and CuOEP ($\tau_{T0} = 105$ ns; CuOEP = 2,3,7,8,12,13,17,18-octaethylporphyrinatocopper(II)).[10] The phosphorescent nature of CuDAP is in marked contrast to the nonphosphorescent nature of CuP at room temperature, indicating that the lifetime difference is due to a slow nonradiative decay rate (k_{nr}) of CuDAP. This is not attributable to the energy gap law in the nonradiative transition[14,15] since the energy levels of the T_1 state of **1a–c** are lower than those of CuTPP and CuOEP. In addition, the thermal activation from the $^4T_1$ to the $^2T_1$ state is not an important bottleneck for the overall relaxation of the T_1 state of CuDAP because the ΔE_T value of **1a** is comparable to or smaller than those of CuPs ($\Delta E_T = 310$–$600\ cm^{-1}$), and also because the spin densities on the Cu atom of 10,20-diphenyl-CuDAP (**1m**) and CuTPP, estimated by density functional theory (DFT) calculations, are almost the same (ca. 0.65; Figure S6).[16]

The introduction of the two N_{meso} atoms gives rise to the T_1 state with an electronic configuration of $|d_{x^2-y^2}a_u b_{3g}|$, where the $d_{x^2-y^2}$, a_u, and b_{3g} orbitals are respectively the SOMO of Cu, the HOMO of DAP, and the LUMO of DAP (Figure S6).[17] The configuration of $|d_{x^2-y^2}a_u b_{3g}|$, in which the a_u orbital has negligible electron density on the four N_{core} atoms, is consistent with the relatively small ΔE_T of **1a**. The direct vibronic coupling between the $^2[d_{x^2-y^2}a_u b_{3g}]$ and the $^2S_0$ states of CuDAP can be promoted by vibrations with the b_{3u} mode. It should be pointed out that vibrational modes accompanied with out-of-plane bending of *meso*-substituents in CuPs[10,18] and torsional librations of the *meso*-phenyl groups leading to nonplanar distortions in OEPs[19] play an important role for the nonradiative decay from the T_1 state. No atom nor group bonding to the two N_{meso} atoms in CuDAP would effectively reduce the vibronic coupling induced by the b_{3u} vibrational modes, e.g. wagging of the *meso*-substituents including out-of-plane skeleton deformation.[20] The rigid molecular structure around the N_{meso} atoms in CuDAP (Figure S6), which is suggested from the short N_{meso}–C_α bond length of **1m** (1.325 Å) compared with the C_{meso}–C_α bond length of CuTPP (1.398 Å), changes the frequency of b_{3u} wagging of the macrocycle accompanied by the out-of-plane

bending deformation[20] so that it may also be a possible factor to decrease the nonradiative decay of CuDAP.

3. Conclusion

We established an alternative method for the synthesis of 10,20-diaryl-CuDAPs from 5-aryl-1,9-dichlorodipyrrins, β-alanine alkyl esters, and $Cu(OAc)_2$, using metal-templated cyclization and *N*-dealkylation reactions as the key steps. The effect of the β-substituents on the optical HOMO–LUMO gaps of CuDAP was stronger than that of the *meso*-aryl groups. The electronic effect of the *meso*-aryl groups on the triplet lifetime and $^1O_2$-generation quantum efficiency of CuDAP was relatively weak, whereas that of the β-(1-pyrazolyl) groups was appreciable, which can be explained by considering the characteristics of the HOMO and LUMO of the DAP ring and the T_1–S_0 energy gaps. The analysis of the temperature dependence of phosphorescence spectra and excited state dynamics of 10,20-dimesityl-CuDAP revealed that the energy gap between the $^4T_1$ and the $^2T_1$ states (ΔE_T = ca. 280 cm^{-1}) is close to the activation energy ($E_a = 310\ cm^{-1}$) for the decay of the $^2T_1$ state, reflecting the efficient reverse intersystem crossing from the $^4T_1$ to the $^2T_1$ state. It is probable that the two N_{meso} atoms with no peripheral substituent as well as the rigid molecular structure around the N_{meso} atoms play a crucial role in decreasing the nonradiative decay rate from the T_1 states of CuDAPs compared with that of CuPs. The present findings provide a guideline for chemically tuning the photophysical properties of CuDAP for future applications.

4. Experimental

General. All melting points were recorded on a Yazawa micro melting point apparatus and are uncorrected. ^1H and $^{13}C\{^1H\}$ NMR spectra were recorded on an Agilent or Bruker 400 MHz spectrometer using $CDCl_3$ as a solvent. Chemical shifts are reported in ppm as relative values vs. tetramethylsilane. The NMR spectra are shown in Figures S7–S14. High-resolution ESI mass spectra were obtained on a Thermo Fisher Scientific EXACTIVE spectrometer. IR (Attenuated Total Reflection; ATR) spectra were obtained on a JASCO FT/IR4600 spectrometer. UV–vis–NIR absorption spectra were measured on a JASCO V-530 spectrometer. Electrochemical measurements were performed on a CH instruments model 650E electrochemical workstation using a glassy carbon working electrode, a platinum wire counter electrode, and an Ag/Ag^+ [0.01 M $AgNO_3$, 0.1 M Bu_4NPF_6 (MeCN)] reference electrode. Scan rate was 60 mV s^{-1}, and the potentials were calibrated with ferrocene/ferrocenium. Chemicals and solvents were of reagent grade quality and used without further purification unless otherwise noted. Thin-layer chromatography was performed with Kieselgel 60 F254, and preparative column chromatography was performed using Silica Gel 60 spherical, neutrality. All reactions were performed under an argon or nitrogen atmosphere.

Synthesis of 4aA. A mixture of **2a** (175 mg, 0.528 mmol), **3A** (694 mg, 3.85 mmol), Et_3N (0.73 g, 7.2 mmol), and MeCN (6 mL) was stirred at 50 °C. After 26 h, CH_2Cl_2 and water were added, and the combined organic extracts were washed with brine and dried over Na_2SO_4 to leave a solid residue, which was purified on a silica-gel column (hexane/AcOEt; 10:1) to afford **4aA** as a red oil (152 mg, 73%).

Synthesis of 5aA. A mixture of **4aA** (129 mg, 0.324 mmol), $Cu(OAc)_2$ (58.7 mg, 0.323 mmol), CH_2Cl_2 (8 mL), and MeOH (8 mL) was stirred at room temperature. The progress of reaction was monitored by TLC and UV-vis spectroscopy. After **4aA** was consumed, an aqueous solution of KPF_6 was added, and the mixture was vigorously stirred. The organic phase was separated, dried over Na_2SO_4, and purified on a silica-gel column (CH_2Cl_2/MeOH; 40:1) to afford **5aA** as a green solid (113 mg, 77%) after recrystallization from CH_2Cl_2–Et_2O.

Synthesis of 1a. A mixture of **5aA** (84 mg, 0.091 mmol), NaOH (78 mg, 2.0 mmol), EtOH (10 mL), and H_2O (13 mL) was stirred at 60 °C. The progress of reaction was monitored by TLC and UV-vis spectroscopy. After 22 h, an aqueous HCl solution was added to neutralize the mixture, and the aqueous layer was extracted with CH_2Cl_2. The combined organic extracts were washed with brine, dried over Na_2SO_4, and concentrated under reduced pressure to leave a solid residue, which was recrystallized from CH_2Cl_2–hexane to afford **1a** as a purple solid (23 mg, 42%) in a high state of purity.

Selected X-ray Crystallographic Data. Single crystals of **5cA** were grown from CH_2Cl_2–CH_3OH. Crystallographic data reported in this manuscript have been deposited with Cambridge Crystallographic Data Centre as supplementary publication no. CCDC-2130982. Copies of the data can be obtained free of charge via CCDC Website. Selected parameters: $C_{42}H_{36}CuF_6N_6O_8P$, MW = 961.28, 0.010 × 0.010 × 0.010 mm, monoclinic, $P2_1/c$, $a = 13.739(3)$ Å, $b = 16.757(3)$ Å, $c = 16.724(4)$ Å, $\beta = 91.416(4)°$, $V = 3849.0(14)$ $Å^3$, $Z = 4$, $\rho_{calcd} = 1.659\ g\ cm^{-3}$, $\mu = 1.75\ cm^{-1}$, collected 86510, independent 8731, parameters 581, $R_w = 0.0995$ (all data), $R_1 = 0.0355$ ($I > 2.0\sigma(I)$), GOF = 1.051.

Measurement of Transient Absorption and Phosphorescence. Nanosecond transient absorption spectroscopy was carried out with setup described elsewhere.[21] Briefly, the second harmonics from a Nd:YAG laser (Continuum Minilite, duration of 10 ns, power of 0.5 mJ/pulse, repetition of 10 Hz) and white continuous light from a 75 W xenon lamp (OBB Power Arc) were used as pump and probe light sources, respectively. The probe light passing through the sample solution in a 1 cm quartz cuvette was dispersed with a monochromator (Spectral Products CM110) and detected with a photomultiplier tube (Hamamatsu R955). The sample solutions were bubbled with Ar gas for 15 min and sealed with a rubber cap before the measurement. After the measurement in the Ar-saturated condition, the solutions were bubbled with air and sealed with a rubber cap for the measurement in the air-saturated condition. The laser power of 0.5 mJ/pulse was low enough that contributions of bimolecular processes on the lifetimes of the triplet excited CuDAPs were negligible. Near infrared phosphorescence signals were detected with the same apparatus for the transient absorption measurement except that an InGaAs or a Si PIN photodiode detector was used, and the probe light was not applied.

Measurement of $^1O_2$ Generation Efficiency. A mixture of sensitizer (Abs = 0.2 at 540 nm), 1,3-diphenylisobenzofuran (DPBF; 90 μM), and toluene (2 mL) was stirred in a quartz cell at 20 °C. The apparatuses used for the irradiation were the same as those reported in ref 5a. The consumption of DPBF was

monitored by absorption decay at 411 nm (Figure S4). The relative quantum yields of $^1O_2$ generation were determined by comparison with the reported value for ZnTPP (94%).[22]

This work was supported by JSPS KAKENHI (Grant Numbers: 18H01961, 21H04576 to YM; 18K05036, 21K04980 to HN, and 19K05399 to TM) and the Research Program of "Five-star Alliance" in "NJRC Mater. & Dev." (20214029), a research grant of The Foundation for Japanese Chemical Research (492(R)) to TI. We would also like to express our gratitude to the SPring-8 synchrotron facility, where synchrotron-radiation experiments were performed at the BL02B1 beamlines with the approval of the Japan Synchrotron Radiation Research Institute (JASRI) under proposal numbers 2020A0557, 2020A0834, 2020A1056, 2020A1644, 2020A1656, and 2021A1592.

Supporting Information

The other experimental details, DFT calculations, characterization data, and spectra for new compounds are available in the Supporting Information on https://doi.org/10.1246/bcsj.20220002.

References

1 For example, see: a) S. Singh, A. Aggarwal, N. V. S. D. K. Bhupathiraju, G. Arianna, K. Tiwari, C. M. Drain, *Chem. Rev.* **2015**, *115*, 10261. b) S. Monro, K. L. Colón, H. Yin, J. Roque, III, P. Konda, S. Gujar, R. P. Thummel, L. Lilge, C. G. Cameron, S. A. McFarland, *Chem. Rev.* **2019**, *119*, 797.

2 a) H. Shinmori, F. Kodaira, S. Matsugo, S. Kawabata, A. Osuka, *Chem. Lett.* **2005**, *34*, 322. b) S. Satake, H. Shinmori, S. Kawabata, K. Sugikawa, H. Funabashi, A. Kuroda, A. Ikeda, *Org. Biomol. Chem.* **2019**, *17*, 3141.

3 J.-F. Longevial, A. Yamaji, D. Aggad, G. Kim, W. X. Chia, T. Nishimura, Y. Miyake, S. Clément, J. Oh, M. Daurat, C. Nguyen, D. Kim, M. Gary-Bobo, S. Richeter, H. Shinokubo, *Chem. Commun.* **2018**, *54*, 13829.

4 T. Sugai, M. Minoura, H. Nakano, Y. Matano, *Bull. Chem. Soc. Jpn.* **2018**, *91*, 1264.

5 a) S. Omomo, T. Sugai, M. Minoura, H. Nakano, Y. Matano, *Angew. Chem., Int. Ed.* **2018**, *57*, 3797. b) S. Omomo, R. Fukuda, T. Miura, T. Murakami, T. Ikoma, Y. Matano, *ChemPlusChem* **2019**, *84*, 740.

6 a) J. Mack, N. Kobayashi, *Chem. Rev.* **2011**, *111*, 281. b) Y. Matano, *Chem. Rev.* **2017**, *117*, 3138.

7 a) R. L. N. Harris, A. W. Johnson, I. T. Kay, *J. Chem. Soc. C* **1966**, 22. b) O. G. Khelevina, N. V. Chizhova, P. A. Stuzhin, A. S. Semeikin, B. D. Berezin, *Russ. J. Coord. Chem.* **1996**, *22*, 811. c) Y. Matano, T. Shibano, H. Nakano, H. Imahori, *Chem.—Eur. J.* **2012**, *18*, 6208. d) Y. Matano, T. Shibano, H. Nakano, Y. Kimura, H. Imahori, *Inorg. Chem.* **2012**, *51*, 12879.

8 a) M. Mutoh, K. Sudoh, K. Furukawa, M. Minoura, H. Nakano, Y. Matano, *Asian J. Org. Chem.* **2019**, *8*, 352. b) Y. Shimizu, Y. Matano, *J. Porphyr. Phthalocyanines* **2021**, *25*, 1004.

9 In both mechanisms, the base-promoted reaction (deprotonation or hydrolysis) should be a rate-determining step. For details, see: Scheme S1.

10 M. Asano, Y. Kaizu, H. Kobayashi, *J. Chem. Phys.* **1988**, *89*, 6567.

11 For example, see: a) B. E. Smith, M. Gouterman, *Chem. Phys. Lett.* **1968**, *2*, 517. b) D. Eastwood, M. Gouterman, *J. Mol. Spectrosc.* **1969**, *30*, 437. c) D. Kim, D. Holten, M. Gouterman, *J. Am. Chem. Soc.* **1984**, *106*, 2793. d) J. A. S. Cavaleiro, H. Görner, P. S. S. Lacerda, J. G. MacDonald, G. Mark, M. G. P. M. S. Neves, R. S. Nohr, H.-P. Schuchmann, C. von Sonntag, A. C. Tomé, *J. Photochem. Photobiol., A* **2001**, *144*, 131. e) E. I. Sagun, É. I. Zen'kevich, V. N. Knyukshto, A. M. Shul'ga, *Opt. Spectrosc.* **2005**, *99*, 731. f) H. Marcille, J.-P. Malval, M. Presset, N. Bogliotti, A. Blacha-Grzechnik, V. Brezová, Y. Yagci, D.-L. Versace, *Polym. Chem.* **2020**, *11*, 4237, and references therein.

12 In ref. 10, the phosphorescence lifetimes of four Cu^{II} porphyrins were reported to be 17–105 ns in toluene at 300 K. In ref. 11f, the phosphorescence lifetime of Cu^{II} 5,15-diphenylporphyrin was reported to be 50 ns in 2-methyl-THF at 77 K.

13 The phosphorescence lifetimes of Zn^{II} 3,7,13,17-tetraethyl-2,8,12,18-tetramethyl-5,15-diazaporphyrin (diazaetioporphyrin II) and Zn^{II} 2,7,12,17-tetraethyl-3,8,13,18-tetramethylporphyrin (etioporphyrin I) were reported to be 16 ms and 57 ms, respectively, in diethyl ether–petroleum ether (1:1) at 77 K. See: S. S. Dvornikov, V. N. Knyukshto, V. A. Kuzmitsky, A. M. Shulga, K. N. Solovyov, *J. Lumin.* **1981**, *23*, 373.

14 R. Englman, J. Jortner, *Mol. Phys.* **1970**, *18*, 145.

15 S. J. Jang, *J. Chem. Phys.* **2021**, *155*, 164106.

16 In our previous report (ref. 5b), we proposed that the relatively short N_{meso}–C_α bond length of **1a** would cause the increase in ΔE_T compared with that of CuTPP. However, this interpretation has been contradicted by the present experimental results.

17 The combination of the LUMO (b_{3g}) and the HOMO (a_u) of DAP with the close-lying SOMO ($d_{x^2-y^2}$) of Cu makes the electronic configuration of the T_1 state for CuDAP.

18 M. Asano-Someda, Y. Kaizu, *J. Photochem. Photobiol., A* **1995**, *87*, 23.

19 V. Knyukshto, E. Zenkevich, E. Sagun, A. Shul'ga, S. Bachilo, *Chem. Phys. Lett.* **1998**, *297*, 97.

20 M. Aydin, *Vib. Spectrosc.* **2013**, *68*, 141.

21 T. Miura, K. Maeda, Y. Oka, T. Ikoma, *J. Phys. Chem. B* **2018**, *122*, 12173.

22 W. Spiller, H. Kliesch, D. Wöhrle, S. Hackbarth, B. Röder, G. Schnurpfeil, *J. Porphyr. Phthalocyanines* **1998**, *2*, 145.